Published in final edited form as:
Polyhedron. 2013 July 13; 58: 134–138. doi:10.1016/j.poly.2012.08.079.

Kinetics of CO Recombination to the Heme in *Geobacillus Stearothermophilus* Nitric Oxide Synthase†

Charlotte A. Whited, **Jeffrey J. Warren**, **Katherine D. Lavoie**, **Jay R. Winkler***, and **Harry B. Gray***
Beckman Institute, California Institute of Technology, Pasadena, CA 91125

Abstract

We report the kinetics of CO rebinding to the heme in His134Ser, Ile223Val and His134Ser/Ile223Ser mutants of *Geobacillus stearothermophilus* nitric oxide synthase (gsNOS). The amplitudes of the two observed kinetics phases, which are insensitive to CO concentration, depend on enzyme concentration. We suggest that two forms of gsNOS are in equilibrium under the conditions employed (6.1–27 μM gsNOS with 20 or 100% CO atmosphere). The kinetics of CO rebinding to the heme do not depend on the identity of the NO-gate residues at positions 134 and 223.

Keywords

Nitric oxide synthase; carbon monoxide; heme proteins

1. Introduction

Michelle Millar made major contributions to the understanding of iron-sulfur bonding in biological molecules [1,2]. She also was interested in blue copper proteins [3], cytochromes P450 [4] and nitric oxide synthases (NOS) [5]. In this tribute to her, we report investigations of photoinitiated carbon monoxide (CO) release and rebinding to the heme in the nitric oxide synthase from *Geobacillus stearothermophilus* (gsNOS).

Nitric oxide (NO) is an important signaling molecule in all eukaryotes [6–9] and may be used by prokaryotes to combat host immune response [10–12]. The enzyme (NOS) produces NO [5,13] in a catalytic cycle in which the first turnover involves two-electron oxidation of arginine to *N*-hydroxy-L-arginine. Then, in a second turnover, a one-electron oxidation converts *N*-hydroxy-L-arginine to L-citrulline and heme-bound NO. How the protein controls the rate of NO release in the various forms of NOS enzymes is not fully understood.

The 200-fold difference in NO-release rates between bacterial and mammalian enzymes [14] is striking, particularly in view of high sequence similarities and conserved folds among NOS isoforms. Crystallographic studies suggest that Val is the first gate for NO release in mammalian enzymes (e.g. Val396 in human endothelial NOS [15,16]); bacterial

†In memory of Michelle Millar.

winklerj@caltech.edu, hbgray@caltech.edu, Tel: (626) 395-6500, Fax: (626) 449-4159.

homologues have Ile resides at the analogous position (based on α-carbon overlays) [7,17]. Stuehr and coworkers showed that Val346 → Ile346 mutation in mouse inducible NOS slows NO release, while Ile224 → Val224 substitution in *Bacillus subtilus* NOS increases the reaction rate [18]. Of interest here is that smaller residues at a second gate also promote NO release: for example, neuronal NOS releases NO with a rate constant of 5 s^{-1}, with Val567 at the first gate and Ser477 at the second gate (rat enzyme numbering [19,20]). NOS from *Sorangium cellulosum* NOS has the fastest recorded NO release kinetics (7–10 s^{-1}), where Val1014 and Gly923 are at the two gating positions [21]. We have investigated four site-directed mutants of gsNOS that have different amino acids at the two NO-gate positions, 134 and 223 (Figure 1): wild type (wt), I223V, H134S, and the double mutant H134S/I223V. In single-turnover experiments we found that the rate of NO release in the gsNOS double mutant (1.0 s^{-1}) approached that of fast NO releasing isoforms at 298 K [14]. We have extended our work on these isoforms to include kinetics of CO rebinding to the gsNOS heme.

2. Materials and Methods

Sample preparation

The plasmid for the nitric oxide synthase from *Geobacillus stearothermophilus* was a gift from B. R. Crane (Cornell University). The enzyme was expressed as described previously [22]. Mutations were introduced using the QuikChange site-directed mutagenesis protocol from Stratagene. Primers were designed according to the guidelines outlined by the QuikChange manual. Unless otherwise noted, protein solutions were prepared using 50 mM Tris (2-amino-2-hydroxymethyl-propane-1,3-diol), pH 7.5 and 150 mM NaCl. Steady-state UV-visible spectra were recorded on an Agilent 8453 diode array spectrophotometer.

For laser experiments, oxygen-free samples were pumped into an anaerobic chamber (with an atmosphere of 100% N_2) and reduced using an excess of sodium dithionite ($Na_2S_2O_4$). A small excess $Na_2S_2O_4$ was left in samples to ensure that NOS remained in the ferrous state throughout the course of the experiment. Samples were then placed in a quartz cuvette (Starna Cells) with a graded seal connecting the cuvette to a vacuum stopcock. The cuvettes were sealed and removed from the anaerobic chamber. The side arm of the cuvette was attached to a Schlenk line, evacuated, then backfilled with carbon monoxide (100% CO or 20% CO + 80% N_2) three times. Once the side arm was under the desired atmosphere, the stopcock was opened to the side arm. The headspace of the cuvette, above the protein solution, was evacuated and back-filled with CO from the Schlenk line and sealed under this new atmosphere. The sample shielded from light and was gently shaken over night at 4 °C to allow for full equilibration of the atmosphere with the solution. Inadequate equilibration time resulted in irreproducibility between samples.

Formation of the ferrous-CO complex was confirmed using its characteristic absorption band at 446 nm [23]. The stability of the sample was monitored by UV-visible spectroscopy after its generation, and immediately before and after laser irradiation.

Nanosecond Transient Absorption Spectroscopy

All transient UV-visible spectroscopic measurements were conducted at the Beckman Institute Laser Resource Center at Caltech. Excitation for time-resolved measurements (560 nm, 8-ns) was provided by an optical parametric oscillator (Spectra-Physics Quanta-Ray MOPO-700) pumped by the third-harmonic of a Q-switched Nd:YAG laser (Spectra-Physics Quanta-Ray PRO-Series). The details of this setup have been described [24]. Kinetics traces were collected at 410 and 440 nm for each protein sample; all measurements were made in duplicate.

Data Analysis

Transient absorption traces were fit using Igor-Pro (WaveMetrics Inc., Lake Oswego, OR, USA) graphing software. Traces monitoring the signal over time at a single wavelength were fit to a double exponential function (Eq. 1); residuals were less than 1% of the maximum signal amplitude.

$$y=A_1\exp(-t/\tau_1)+A_2\exp(-t/\tau_2) \quad (1)$$

3. Results

3.1 Steady-state spectroscopy

UV-visible spectroscopy was used to characterize the resting state and to verify that solutions of ferrous protein with added carbon monoxide quantitatively produce ferrous-CO adducts. This technique is particularly informative given the sensitivity of heme absorption bands to their environment, ligation, and oxidation state. Each ferrous-CO enzyme displayed a single Soret maximum (446 nm), as expected for carbon monoxy NOS [23]. The optical spectra of both ferrous and ferrous-CO forms of wt gsNOS are shown in Figure 2. Virtually identical spectra were obtained for the Fe(II) and Fe(II)-CO H134S, I223V and H134S/I223V proteins.

3.2 CO Rebinding Kinetics

Ferrous–CO adducts are commonly used as models of interactions of diatomic molecules with heme proteins [25–27]. Although stable in the dark, the Fe-C bond ruptures when (heme)Fe^{II}-CO is exposed to visible light, producing CO and a five-coordinate ferroheme; under an atmosphere of CO, the six-coordinate Fe(II)-CO complex readily reforms [28]. The large differences in absorption spectra of five- and six-coordinate heme species (Figure 2) greatly facilitate optical monitoring of CO dissociation and rebinding, as documented for myoglobin [28], human myeloperoxidase [29], and cytochrome P450 [26].

Laser-flash excitation (560 nm) of Fe^{II}-CO wt gsNOS produces a transient species with a difference spectrum that closely matches that expected for formation of the five-coordinate ferrous enzyme (Figure 3). Transient absorption monitored at 440 nm [near the maximum absorption of the Fe(II)-CO heme] and 410 nm [near the maximum absorption of the transiently generated Fe(II) form] reveals that a coordinatively unsaturated heme is generated almost instantaneously. The yield of Fe(II)-NOS produced upon irradiation (based on ΔOD_{410}) is independent of the identity of the gate residues at positions 134 and 223. Under a CO atmosphere, the Fe(II)-CO complex reforms on the millisecond timescale (representative data for wt gsNOS are shown in Figure 4; results for the three other mutants are qualitatively similar). CO must escape the heme pocket and diffuse back to the ferrous heme to account for the ms-timescale kinetics [25–27]. The kinetics traces are best described by a biexponential function (Eq. 1); fitting parameters for each sample are given in Table 1.

To probe the origin of the biphasic kinetics, the CO concentration was changed by using a mixture of 20% CO + 80% N_2 (1 atm), which results in approximately a five-fold reduction in both rate constants, consistent with first-order dependences on [CO] (Table 1). The amplitudes of the two kinetics phases were insensitive to [CO].

The rate constant $k_{1,obs}$ is pseudo-first-order under our experimental conditions (6 μM gsNOS + 1 or 0.2 atm CO; 1 atm CO ([CO] ~ 1 mM at 298 K [30]). Second-order rate constants for CO-rebinding were approximated from the two pseudo-first-order rate constants; the constants for the slower kinetics phase were lower than 10^6 M^{-1} s^{-1}, while

those for the fast phase were slightly higher than 10^6 M^{-1} s^{-1}. All of the second-order rate constants are consistent with those for CO-rebinding to the heme in other proteins [32,33]. Notably, there is no clear correlation between CO-rebinding rate constants and the nature of the NO-gating residues at positions 134 and 223.

We also examined the dependence of CO-rebinding kinetics on gsNOS concentration (6.1, 9.9 and 27 μM). Although the rate constants were insensitive to [gsNOS], the relative amplitudes of the two kinetics phases varied by roughly a factor of two, suggesting that two forms of the enzyme, Fe_A and Fe_B, with different CO-binding rates were present in solution.

We note that cooperative or anti-cooperative CO-rebinding to NOS dimers can complicate the kinetics analysis [31]. Photodissociation of CO is an efficient process, which could, in principle, produce populations of CO-dissociated monomers and singly or doubly CO-dissociated dimers. A ten-fold increase in laser power did not alter the ratio of the two observed rate constants, nor their relative amplitudes; however, the signal strength increased with increasing laser power.

4. Discussion

Bimolecular recombination of CO to a protein-encapsulated ferroheme (k_1, Scheme 1) typically occurs with rate constants $k_1 \sim 10^5$ to 10^6 M^{-1} s^{-1}, roughly independent of the size of the protein (e.g. wt myoglobin: 6.5×10^5 [32]; wt cytochrome $P450_{nor}$: 6.1×10^5 M^{-1} s^{-1} [33]). Geminate recombination to Fe(II) (k_{gem}, Scheme 1), which occurs when CO does not escape the heme pocket [34] is very rapid and is not usually observed using experimental conditions similar to ours [28,35]. Thus, under pseudo-first-order conditions of excess CO, the recombination kinetics are expected to be monoexponential.

Scheme 1 cannot account for the two discrete CO-rebinding phases as there must be two forms of gsNOS in solution, denoted Fe_A and Fe_B in Scheme 2. The rate constants k_1 and k_2 are for CO-rebinding to Fe_A and Fe_B, respectively. Interconversion of Fe_A and Fe_B must be slower than CO-rebinding to account for the observed kinetics. We note that residues at gsNOS NO-gate positions 134 and 223 only slightly affect the amplitudes in Table 1, in contrast to results from single-turnover NO release experiments [14]. Biphasic kinetics also were observed for CO-rebinding in mouse inducible NOS [36] and neuronal NOS [37]. The ratios of k_1 and k_2 depend on the NOS variant, as well as the presence of substrate, inhibitor and/or redox cofactor (e.g.; tetrahydrobiopterin). Our results suggest that the origin of the observed population heterogeneity in CO-rebinding could arise from protein concentration, at least for bacterial NOS. At this time we cannot identify the two NOS populations.

We also note that the identities of the residues at gsNOS positions 134 and 223 slightly affect K_{eq} (from the amplitudes in Table 1). This observation is not in clear accord with a monomer/dimer equilibrium because these mutations are far from the putative dimer interface (Figure 1). Regardless of the origin population heterogeneity, the bimolecular CO-heme recombination rates (Table 1) are in a normal range for heme proteins in both proposed gsNOS states.

Our results for CO-rebinding to the heme in mutants of gsNOS contrast with those for NO-release in single-turnover experiments [14]. In the NO-release study we demonstrated the importance of NO-gates at positions 134 and 223. CO-rebinding apparently occurs by other mechanisms, or pathways, that are not dramatically influenced by residues that strongly affect NO release. CO is classically used as an inert model for gas diffusion through proteins, but clearly is not a good model for NO-release in NOS.

One interpretation of the results for CO-rebinding is that NOS enzymes are optimized for extrusion, not (re)binding, of dipolar diatomic gases. This also is supported by slightly faster binding of O_2 versus CO/NO in ferrous neuronal NOS [38] and inducible NOS_{ox} [39], respectively, although this is a crude comparison. We note that NO and CO have similar dipole moments [40,41] and are almost the same size. Alternatively, NO/CO release could occur via a single restricted path, while rebinding could occur by multiple paths. This scenario is consistent with the weak influence of the NO-gate positions on the kinetics of CO-rebinding to the heme. Further, NOS function relies on O_2 diffusion to the heme, suggesting that there are other gas diffusion pathways available.

It is important to point out that the conditions for CO-rebinding experiments are slightly different from those of single-turnover experiments; CO-rebinding experiments were performed in the absence of substrate and the tetrahydrobiopterin cofactor necessary for redox catalysis. The presence of substrate in the active site is known to perturb the active site of NOS [42,43], but it is not known how (or if) these changes modulate gas diffusion behavior, or if the presence of substrate/cofactors influences gsNOS dynamics. It would be of interest to explore how the presence of substrate and cofactors influences CO-rebinding kinetics, which could have broad implications for NOS function.

5. Conclusions

Investigation of CO rebinding to the heme in gsNOS is consistent with the presence of two enzyme populations. Our study suggests the biphasic CO-rebinding kinetics in gsNOS depend on enzyme concentration. We conclude that high CO concentrations can obscure fine details of gas diffusion in and out of the heme active sites, so single-turnover experiments likely will be better probes of *in vivo* reactivity patterns in substrate-releasing enzymes [14].

Acknowledgments

Our work was supported by NIH (DK019038 to HBG and JRW) and (GM095037 to JJW).

References

1. O'Sullivan T, Millar MM. J. Am. Chem. Soc. 1985; 107:4096–4097.
2. Jiang J, Maruani M, Solaimanzadeh J, Lo W, Koch SA, Millar M. Inorg. Chem. 2009; 48:6359–6361. [PubMed: 20507106]
3. Gray HB, Malmström BG, Williams RJP. J. Biol. Inorg. Chem. 2000; 5:551–559. [PubMed: 11085645]
4. Denisov IG, Makris TM, Sligar SG, Schlichting I. Chem. Rev. 2005; 105:2253–2277. [PubMed: 15941214]
5. Rosen GM, Tsai P, Pou S. Chem. Rev. 2002; 102:1191–1200. [PubMed: 11942793]
6. Marletta MA. J. Biol. Chem. 1993; 268:12231–12234. [PubMed: 7685338]
7. Crane BR, Sudhamsu J, Patel BA. Annu. Rev. Biochem. 2010; 79:445–470. [PubMed: 20370423]
8. Stuehr DJ, Santolini J, Wang Z-Q, Wei C-C, Adak S. J. Biol. Chem. 2004; 279:36167–36170. [PubMed: 15133020]
9. Alderton WK, Copper CE, Knowles RG. Biochem. J. 357:593–615. [PubMed: 11463332]
10. Gusarov I, Starodubtseva M, Wang Z-Q, McQuade L, Lippard SJ, Stuehr DJ, Nudler E. J. Biol. Chem. 2008; 283:13140–13147. [PubMed: 18316370]
11. Gusarov I, Shatalin K, Starodubtseva M, Nudler E. Science. 2009; 325:1380–1384. [PubMed: 19745150]
12. Johnson EG, Sparks JP, Dzikovski B, Crane BR, Gibson DM, Loria R. Chem. Biol. 2008; 15:43–50. [PubMed: 18215772]

13. Stuehr D, Pou S, Rosen GM. J. Biol. Chem. 2001; 276:14533–14536. [PubMed: 11279231]
14. Whited CA, Warren JJ, Lavoie KD, Weinert EE, Agapie T, Winkler JR, Gray HB. J. Am. Chem. Soc. 2011; 134:27–30. [PubMed: 22148177]
15. Fischmann TO, Hruza A, Niu XD, Fossetta JD, Lunn CA, Dolphin E, Prongay AJ, Reichert P, Lundell DJ, Narula SK, Weber PC. Nat. Struct. Mol. Biol. 1999; 6:233–242.
16. The numbering of the NO-gate residues in the different NOS isoforms corresponds to the numbering system for each respective enzyme. UniProtKB ID: Q5KZC5, gsNOS; P29476, rat neuronal NOS; P29477, mouse inducible NOS; P29474, human endothelial NOS; A9FD96, *Sorangium cellulosum* NOS; O34453, *Bacillus subtilus* NOS.
17. Sudhamsu J, Crane BR. Trends Microbiol. 2009; 17:212–218. [PubMed: 19375324]
18. Wang Z-Q, Wei C-C, Sharma M, Pant K, Crane BR, Stuehr DJ. J. Biol. Chem. 2004; 279:19018–19025. [PubMed: 14976216]
19. Zhang J, Martásek P, Paschke R, Shea T, Masters BSS, Kim J-JP. J. Biol. Chem. 2001; 276:37506–37513. [PubMed: 11473123]
20. Zhou L, Zhu DY. Nitric Oxide-Biol. Chem.. 2009; 20:223–230.
21. Agapie T, Suseno S, Woodward JJ, Stoll S, Britt RD, Marletta MA. Proc. Natl. Acad. Sci. U.S.A. 2009; 106:16221–16226. [PubMed: 19805284]
22. Sudhamsu J, Crane BR. J.Biol. Chem. 2006; 281:9623–9632. [PubMed: 16407211]
23. Doukov T, Li H, Soltis M, Poulos TL. Biochemistry. 2009; 48:10246–10254. [PubMed: 19791770]
24. Dempsey JL, Winkler JR, Gray HB. J. Am. Chem. Soc. 2009; 132:1060–1065. [PubMed: 20043639]
25. Phillips GN Jr, Teodoro ML, Li T, Smith B, Olson JS. J. Phys. Chem. B. 1999; 103:8817–8829.
26. McLean MA, Yeom H, Sligar SG. Biochimie. 1996; 78:700–705. [PubMed: 9010598]
27. Migita CT, Matera KM, Ikeda-Saito M, Olson JS, Fujii H, Yoshimura T, Zhou H, Yoshida T. J. Biol. Chem. 1998; 273:945–949. [PubMed: 9422754]
28. Austin RH, Beeson KW, Eisenstein L, Frauenfelder H, Gunsalus IC. Biochemistry. 1975; 14:5355–5373. [PubMed: 1191643]
29. Murphy EJ, Maréchal A, Segal AW, Rich PR. Biochemistry. 2010; 49:2150–2158. [PubMed: 20146436]
30. Cargill, RW., editor. IUPAC Solubility Data Series. Vol. Vol. 43. Oxford, England: Carbon Monoxide, Pergamon Press; 1990.
31. Perrella M. Biophys. Chem. 1999; 81:157–178. [PubMed: 10535099]
32. Cao W, Ye X, Sjodin T, Christian JF, Demidov AA, Berezhna S, Wang W, Barrick D, Sage JT, Champion PM. Biochemistry. 2004; 43:11109–11117. [PubMed: 15323570]
33. Shiro Y, Kato M, Iizuka T, Nakahara K, Shoun H. Biochemistry. 1994; 33:8673–8677. [PubMed: 8038156]
34. Gibson QH, Regan R, Elber R, Olson JS, Carver TE. J. Biol. Chem. 1992; 267:22022–22034. [PubMed: 1429552]
35. Doster W, Beece D, Bowne SF, DiIorio EE, Eisenstein L, Frauenfelder H, Reinisch L, Shyamsunder E, Winterhalter KH, Yue KT. Biochemistry. 1982; 21:4831–4839. [PubMed: 7138833]
36. Stevenson TH, Gutierrez AF, Alderton WK, Lian L, Scrutton NS. Biochem. J. 2001; 358:201–208. [PubMed: 11485568]
37. Scheele JS, Kharitonov VG, Martásek P, Roman LJ, Sharma VS, Masters BSS, Magde D. J. Biol. Chem. 1997; 272:12523–12528. [PubMed: 9139703]
38. Abu-Soud HM, Wu C, Ghosh DK, Stuehr DJ. Biochemistry. 1998; 37:3777–3786. [PubMed: 9521697]
39. Abu-Soud HM, Gachhui R, Raushel FM, Stuehr DJ. J. Biol. Chem. 1997; 272:17349–17353. [PubMed: 9211873]
40. Rawlins WT, Person JC, Fraser ME, Miller SM, Blumberg WAM. J. Chem. Phys. 1998; 109:3409–3417.

41. Scuseria GE, Miller MD, Jensen F, Geertsen J. J. Chem. Phys. 1991; 94:6660–6663.
42. Li H, Raman CS, Martásek P, Masters BSS, Poulos TL. Biochemistry. 2001; 40:5399–5406. [PubMed: 11331003]
43. Li H, Igarashi J, Jamal J, Yang W, Poulos T. J. Biol. Inorg. Chem. 2006; 11:753–768. [PubMed: 16804678]

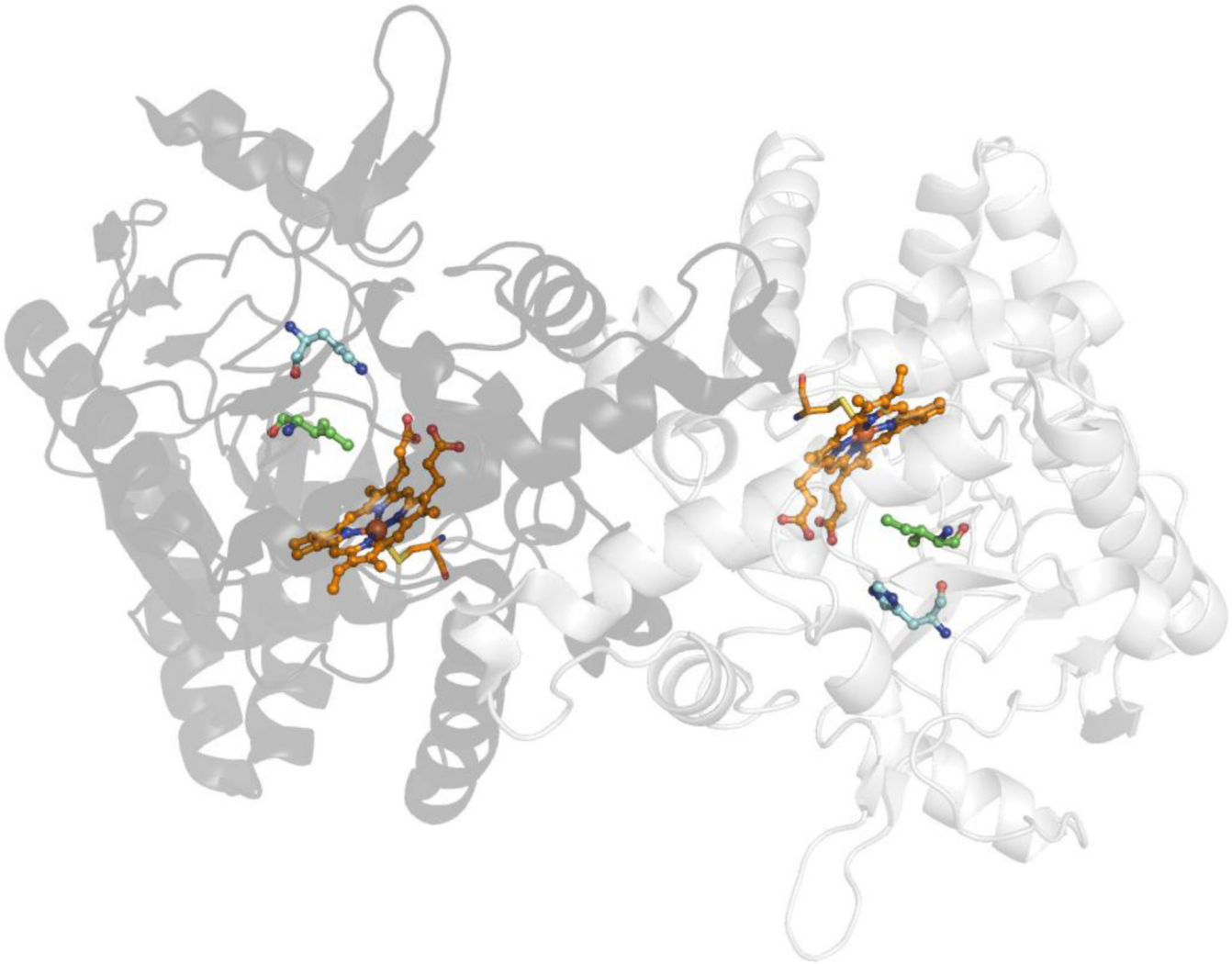

Figure 1.
Structure of wt gsNOS (PDB ID 2FLQ) viewed along the pseudo-C_2 axis. The cysteine-ligated heme is shown in orange: The first NO-gate, Ile134, is in green and the second gate, His223, is in cyan. The two molecules that comprise the dimeric structure are shown in black and gray.

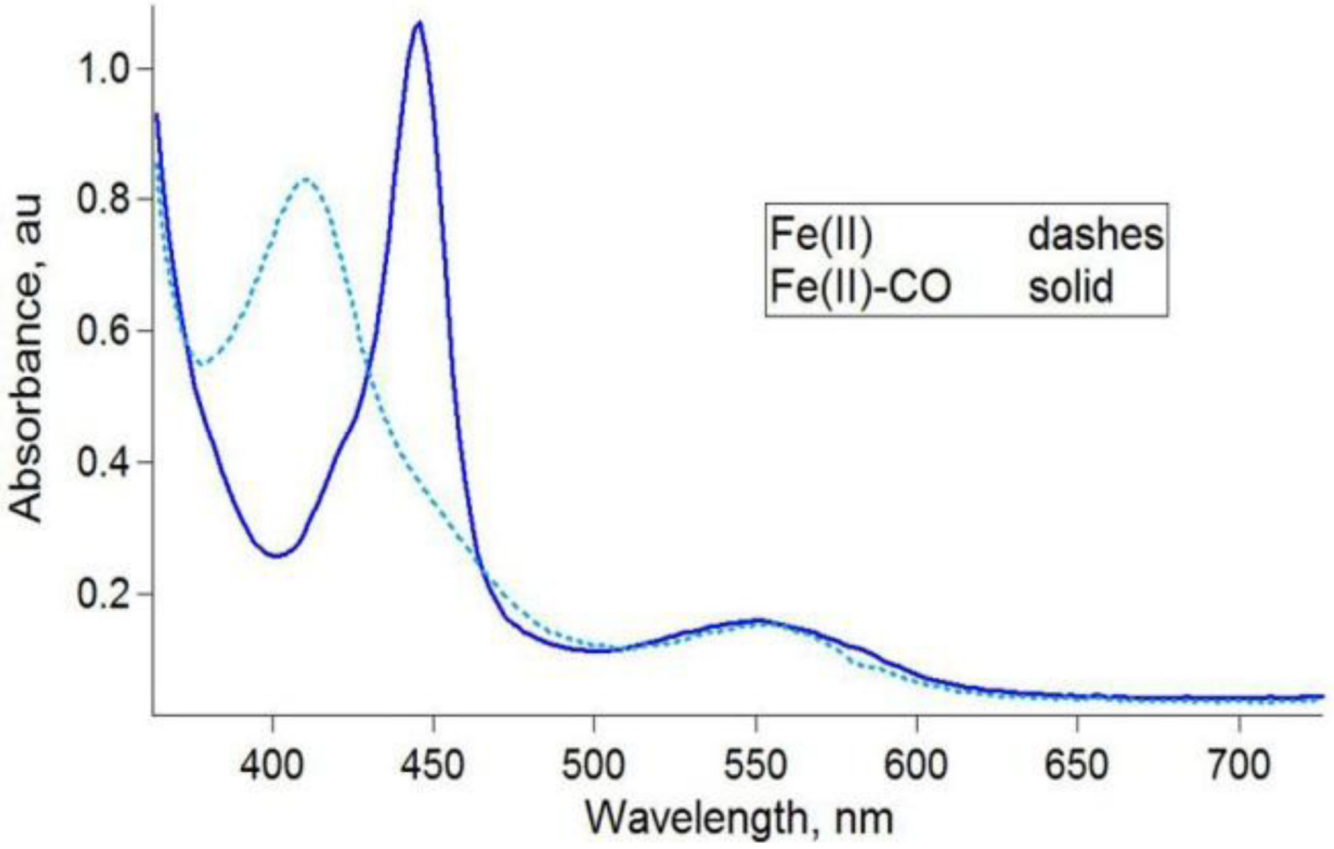

Figure 2.
Absorption spectra of Fe(II) and Fe(II)-CO forms of wt gsNOS.

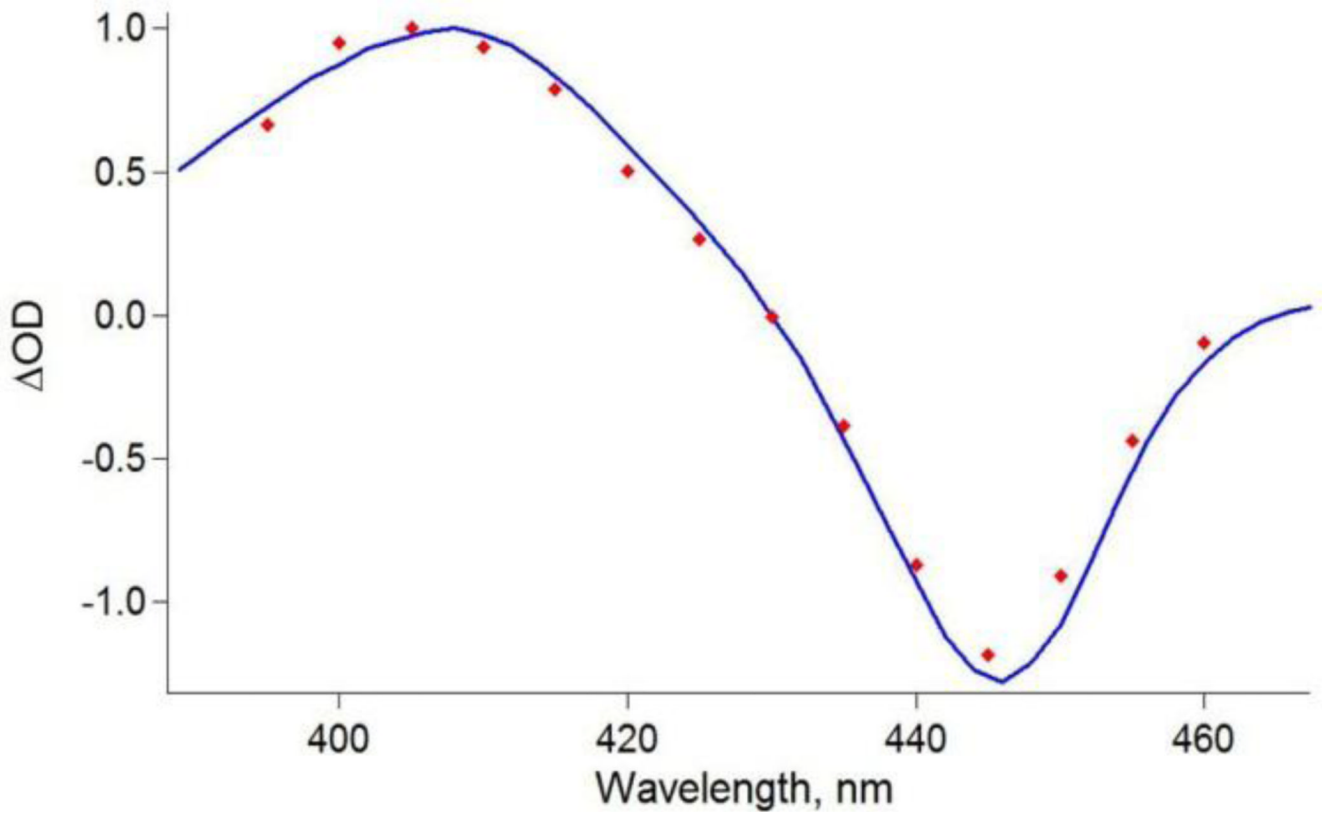

Figure 3.
Scaled steady-state difference spectrum produced by subtracting the spectrum of the wt ferrous-CO complex from the five-coordinate ferrous species (solid blue line) and the transiently generated difference spectrum (red dots, 1 ms after laser pulse, 6.1 μM wt gsNOS).

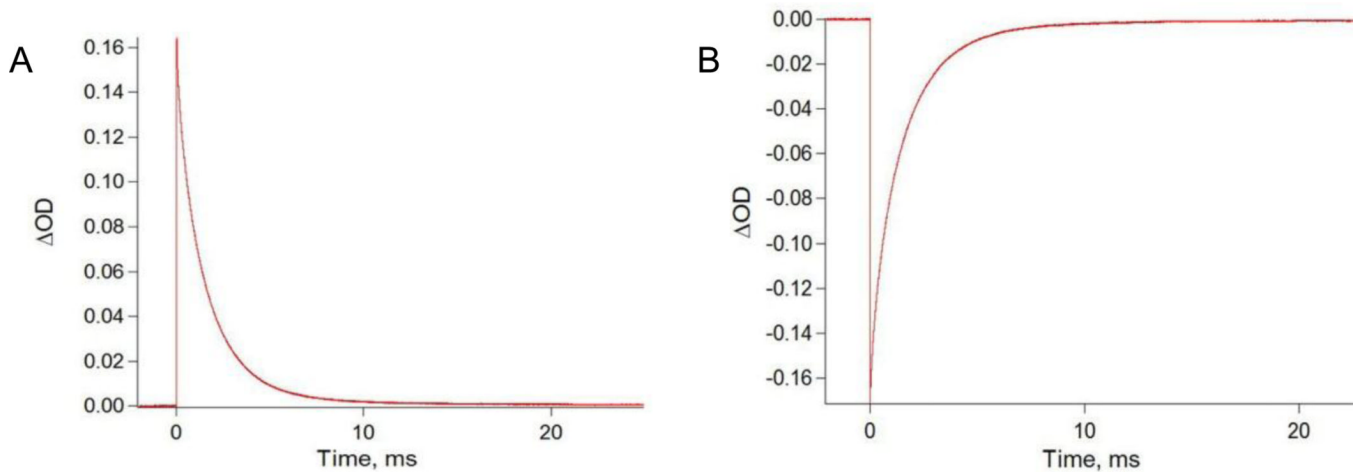

Figure 4.

(A) Typical transient for wt Fe^{II}-CO gsNOS (6.1 μM) under a 100% CO atmosphere recorded at 410 nm following a 560 nm laser pulse and (B) the corresponding bleach/recovery upon loss/rebinding of CO.

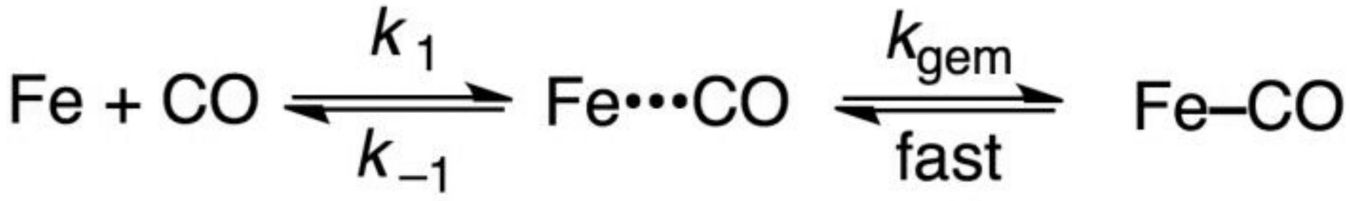

Scheme 1.

Standard kinetics model for the recombination of CO a ferroheme. Fe represents the protein, k_{gem} is the rate constant for geminate recombination and k_1 is the rate constant for bimolecular recombination.

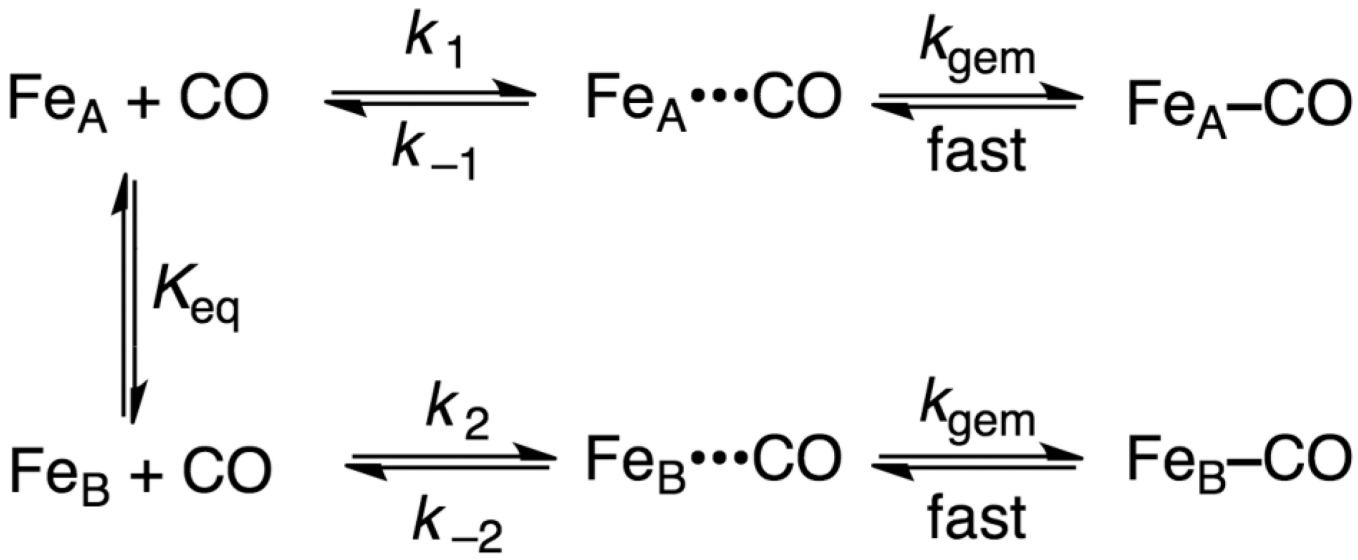

Scheme 2.
Modified kinetics model for the recombination of CO with gsNOS, incorporating the presence of two forms of the enzyme.

Table 1

Rate constants for fast and slow phases of gsNOS/CO recombination. Amplitudes are given at the right of each rate constant.[a]

	wt		I223V		H134S		H134S/I223V	
100% CO								
$k_{1,obs}$ [b]	510	66%	190	46%	750	36%	310	43%
$k_{2,obs}$ [b]	1500	34%	1100	54%	2400	64%	1200	57%
20% CO/80% N_2								
$k_{1,obs}$ [b]	100	60%	45	35%	120	37%	54	51%
$k_{2,obs}$ [b]	390	40%	240	65%	370	63%	240	49%
Second-order rate constants								
$k_{1,bi}$ [c]	5×10^5		2×10^5		8×10^5		3×10^5	
$k_{2,bi}$ [c]	1×10^6		1×10^6		2×10^6		1×10^6	

[a] [gsNOS] = 6.1 μM.

[b] s^{-1}.

[c] $M^{-1}\ s^{-1}$

Table 2

Effects of wt gsNOS concentration on CO-rebinding kinetics.[a]

[gsNOS][b]	$k_{1,obs}$[c]	A_1	$k_{2,obs}$[c]	A_2
6.1	99	64%	400	36%
9.9	110	58%	400	42%
27	91	35%	390	65%

[a] All samples contained an atmosphere of 20% CO + 80% N_2.

[b] μM.

[c] s^{-1}